



Comparative Study Between Stainless Steel and Carbon Steel During Dissimilar Friction Stir Welding with Aluminum: Kinetics of Al–Fe Intermetallic Growth

R. Beygi¹ · R. Carbas¹ · A. Queiros¹ · E. A. S. Marques¹ · R. Shi² · L. F. M. da Silva³

Received: 24 May 2021 / Accepted: 24 June 2021 / Published online: 28 September 2021
© The Korean Institute of Metals and Materials 2021

Abstract

Steel (St) and aluminum (Al) have a high affinity to each other and form intermetallic compounds (IMCs) when bonded by friction stir welding (FSW). Understanding the effect of alloying elements of steel on the formation of IMCs will help to design joints in which the formation of IMCs is controlled. In this study, two kinds of steel, carbon steel (CS) and austenitic stainless steel (SS) with 3 mm thickness, were selected to be welded to aluminum by FSW under similar conditions. The effect of the rotation speed of the FSW tool was also examined in the range of 850–1300 RPM. The morphology, thickness, and composition of IMCs in the interfaces were studied by various characterization techniques. It was observed that the IMC layers in the SS/Al joints were much thinner than the ones in CS/Al joints (0.1–0.7 μm in SS/Al and 2–6 μm in CS/Al). Moreover, the thickness of IMC layer in CS/Al joints increased with increasing the rotation speed while in SS/Al joints it began to decline by exceeding a certain rotation speed. In order to explain these differences, diffusion-based equations were used to calculate the interdiffusion coefficients in both SS/Al and CS/Al couples. It was found that the interdiffusion coefficient in SS/Al was lower than CS/Al. This was attributed to the alloying elements of SS such as Ni and Cr which can diffuse to IMC layer and hinder the growth rate of IMCs. It was also observed that some form of liquation occurred in SS/Al joints at high rotation speed of FSW due to the formation of a low-melting multielement compound of Al–Fe–Cr–Ni. The decline of IMC thickness in SS/Al joints at high rotation speed was attributed to this multielement compound which was melted during FSW and reduced the nucleation rate of Al–Fe IMCs. Finally, the fracture of the specimens and the effect of IMC formation on the joint establishment were elaborated. It was concluded that the alloying elements of steel have a beneficial effect on controlling the growth of IMCs.

Keywords Dissimilar · Welding · Interdiffusion · Nucleation and growth · Alloying elements · Al–Fe · Intermetallics

1 Introduction

The replacement of traditional steel-based construction with lightweight structures made of aluminum is increasing in the automotive industry [1–3]. In addition to weight reduction, there are other advantages found by replacing steel with aluminum. The use of aluminum-steel hybrid structures instead of full steel structures in the front rails of the vehicle increases energy absorption by more than 117% [4]. The quality of the joint determines the performance of Al–St hybrid structures, especially under dynamic loadings [5]. The methods most commonly employed for joining Al–St in the automotive industry are clinching [5], self-piercing riveting [6], and flow drill screwing [7]. Joining by these techniques is mechanical in nature, usually done in an overlap configuration. FSW is a promising method for joining aluminum to steel and has the

✉ R. Beygi
rbeygi@inegi.up.pt

¹ Institute of Science and Innovation in Mechanical and Industrial Engineering (INEGI), 4200-465 Porto, Portugal

² Beijing Advanced Innovation Center for Materials Genome Engineering, University of Science and Technology Beijing, Beijing 100083, China

³ Department of Mechanical Engineering, Faculty of Engineering, University of Porto, 4200-465 Porto, Portugal

advantage that it can be done in butt configuration and can establish metallurgical bonding rather than a mechanical connection [8]. Recently, this process is adopted to be used for joining hard materials such as steel [9]. In contrast to fusion welding processes where a large amount of IMC is generated during welding [10], the IMCs formed in FSW are limited [11]. However, depending on their morphology, even a small amount of IMCs can degrade the joint strength [12]. On the other hand, the existence of IMCs would be an indicative of a joint establishment and guarantees there is a bond between the materials [13].

Among the various Al/St IMCs, the orthorhombic Fe_2Al_5 is more likely to be produced during the FSW process [14]. This phase has a low fracture toughness and tends to generate a brittle fracture [15]. The IMCs not only affect the mechanical properties, but also the corrosion behavior is influenced by their presence [16]. This clarifies even more the importance of controlling the IMCs during the welding process. Since the formation of IMCs is inevitable, the only way to mitigate their adverse effects on joint strength is to control their thickness and morphology [17]. This is most commonly achieved by controlling the heat input [18]. The most straight forward way to achieve this is to control the welding parameters like tool geometry, rotational speed and so on [19, 20]. Using interlayers such as copper or nickel is another alternative to control the growth of IMCs [21]. The effect of welding parameters on IMCs formation during FSW of dissimilar materials has been well studied in the literature [22–25]. In the FSW of the dissimilar Al/St joint, each paper focused primarily on a specific pair of dissimilar metals. Some examples are AA6061/DC04 [26], Al5052/carbon steel [27], AA6061/AISI304 [28], Al5083/DP590 [29], Al6061/ASTM A36 [30] and so on. To the knowledge of the authors, no study is available that compares different pairs of base materials with regards to their effect on the formation of IMCs. In other words, it is not clear whether the alloying elements of a base metal can affect the formation of IMCs during FSW. For example, important differences may arise when an aluminum alloy is friction stir welded to a carbon steel or to a stainless steel. The different heat conductivity of two materials can also influence the thermal history in welding [31] and this may also affect the kinetics of IMCs formation.

The characteristics of the base material, such as crystal structure, microstructure and chemical composition can all influence the growth of IMCs, with the latter having the greatest influence. The influence of alloying elements on IMCs formation is well studied in the literature [32]. Zhang et al. [33] examined the effect of Si and Ge on the thickness of the IMC

layer and concluded that the introduction of Si and Ge reduces the likelihood of reaction and thereby reduces the thickness of the Al–Fe IMC layer. While there are many studies on the effect of alloying elements Al–Fe IMCs formation during fusion based processes [34], this effect has not yet been studied for FSW processes.

This study aims to compare the response of two different kinds of steels during FSW with Al. The purpose is to assess how Al/St IMCs nucleation and growth is affected by base material during FSW. For this purpose, two types of steels, carbon steel and stainless steel, were chosen to be welded to aluminum under identical conditions. In the present study, only the effect of rotation speed is investigated as it is the most important factor in FSW [35]. In both cases, the morphology, thickness, and composition of IMC were examined and compared. Electron microscopy techniques were used to characterize the IMCs at the interface. Tensile tests were performed to assess the joint strength and fracture behavior. Diffusion-based equations and quasi-binary phase diagrams were used to explain the influence of the alloying element on Al/Fe IMCs. Finally, a mechanism was suggested to explain the nucleation and growth mechanism of IMCs during FSW of SS/Al and CS/Al.

2 Experimental Procedure

A 316 stainless steel (SS) and a st37 carbon steel (CS) were chosen to be welded to an Al1050 commercially pure aluminum (Al), each one supplied in 3 mm thick sheets. Table 1 shows the main elements of two types of steels used in this study. AA1050 consists of 99.5 wt% aluminum, with the remainder being composed of Fe and Si.

A H13 tool steel bar was machined to make the FSW tool. Thereafter, a heat treatment was carried out to increase the hardness to 42 HRC. Sheets of steel and aluminum were clamped to the table of the FSW machine. The welding speed was constant and set to 30 mm/min. The tool was plunged in Al. Since a minimum degree of penetration of the tool in St is required to establish the joint [36], an offset of the tool equal to 1 mm was applied towards the steel plate, as shown in Fig. 1a. More detail on the FSW process can be found in a previous work by the authors [12] with the difference that in this study both the pin and shoulder were in rotation. The samples numbering and the corresponding welding condition are listed in Table 2.

Back Scatter Scanning Electron Microscopy (BS SEM) and Energy Dispersive Spectroscopy (EDS) were employed

Table 1 Major elements of CS and SS used here to be joined with Al

Elements (wt%)	C	Mn	P	S	Si	Cr	Ni	Mo
Carbon steel (CS)	0.2	0.75	0.05	0.05	0.3	–	–	–
Stainless steel (SS)	0.08	2	0.045	0.03	0.75	18	14	2

Fig. 1 **a** The schematic of the FSW process and the pin position with respect to the sheets. **b** The position of the tool with respect to both materials. The areas which are marked by black rectangles show the locations of the analyses. **c** The drawing of the tool

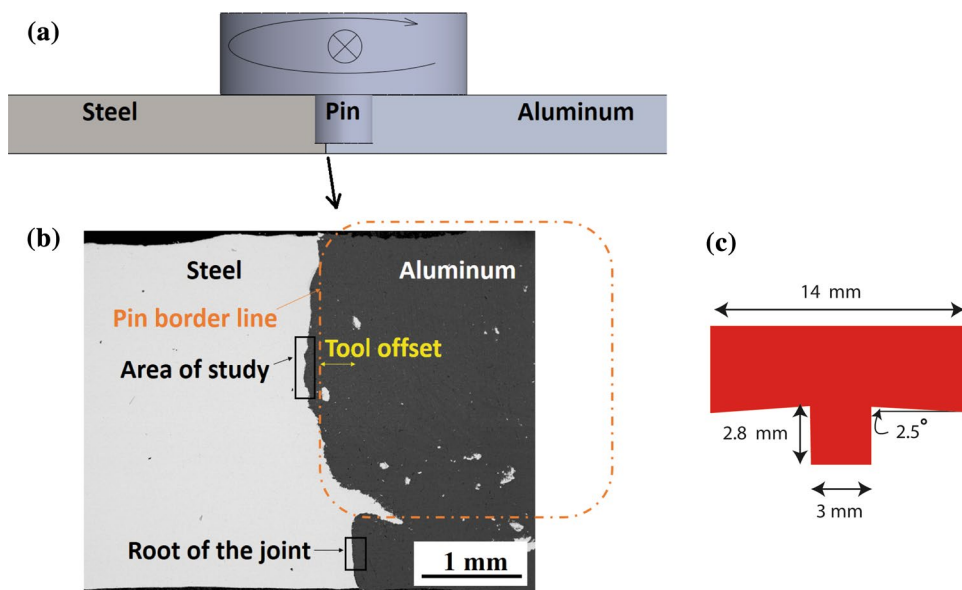


Table 2 The samples numbering, the corresponding welding parameters and the steel types used for obtaining SS/Al and CS/Al joints by FSW

Sample number	Rotation speed (RPM)	Steel type	Welding speed (mm/min)
No. 1	850	SS	30
No. 2	850	CS	30
No. 3	1000	SS	30
No. 4	1000	CS	30
No. 5	1150	SS	30
No. 6	1150	CS	30
No. 7	1300	SS	30
No. 8	1300	CS	30

to characterize the morphology and thickness of IMCs and to accurately measure chemical composition of IMCs. Transmission Electron Microscopy (TEM), High-Resolution Transmission Electron Microscopy (HRTEM) were used to identify the types of IMCs at the interface. These analyses were performed on two locations of the weld interface, the center, and the root, as shown in Fig. 1b. This figure also shows the location of the pin (red dashed line) with respect to two materials. It can be observed that there was not a full penetration of the tool and the root of the joint had no contact with the pin. The drawing of the tool of FSW is also provided in Fig. 1c.

The thickness of IMC layer was measured in several points of each joint using ImageJ software and its average was considered as the thickness of the IMC layer. Two tensile samples were prepared from each welding condition to evaluate the joint strength. The tensile specimens were

prepared according to ASTM E8M standard. The specimens are shown in Fig. 2.

3 Results and Discussion

Since the IMC layer thickness and composition were the most important characteristics considered in the present study, mainly SEM images in backscatter mode and EDS analyses were provided here. In Fig. 3a, b are shown the interface of SS/Al joint (No. 1) in two different magnifications. A thin IMC layer (0.1 μm thickness) is discernible at the interface.

In Fig. 3c, d are shown the SEM images taken from the interface of CS/Al welded joint (No. 2). On the macroscopic scale (Fig. 3c) the interface seems uniform, while on the microscopic scale (Fig. 3d) the IMCs at the interface seem distributed. In this case, the IMC layer thickness is not uniform, and some discontinuities are observed at the interface. The average thickness of IMC in this joint was measured to be 2.1 μm .

In Fig. 4a, b are shown the SEM images from the interface of SS/Al joint (sample 3) taken from 2 different locations. In this figure the IMC layer is more observable than the one shown in Fig. 3a, b. The average thickness of the IMC layer in this sample was 0.2 μm . A hybrid contrast of the IMC layer in Fig. 4b shows that it is composed of two different layers. The element map analysis of the weld interface is shown in Fig. 4c. In addition to Al and Fe, the alloying elements of SS such as Ni, Cr and Mn are also present in the IMC layer. A chemical composition gradient can be seen across the interface, as a color gradient is observed in these regions. Figure 4d, e show the interface of the CS/Al joint (No. 4). A streak of an IMC layer is observed in steel next to



Fig. 2 Tensile specimens prepared from the joints

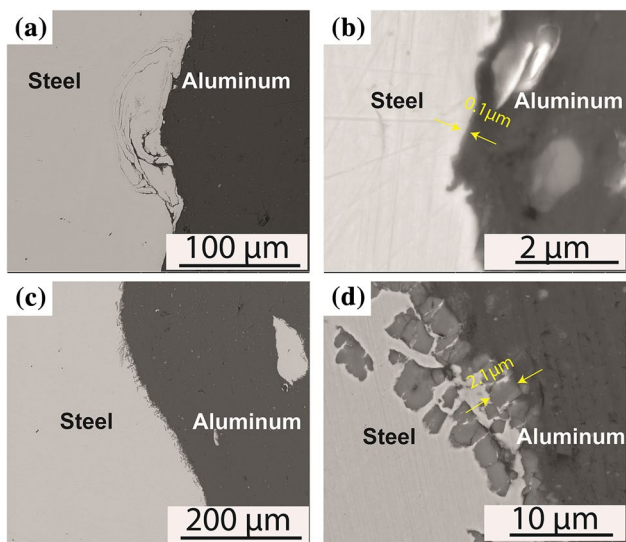


Fig. 3 **a, b** SEM images taken from the interface of SS–Al welded joint (No. 1). **c, d** SEM images taken from the interface of CS–Al welded joint (No. 2). Both joints were made at 850 RPM

the interface. The average thickness of the IMC layer in this sample was 2.5 μm . Some discontinuities are also observed in the interface. The elemental map of the weld interface is shown in Fig. 4f. No color gradient is observed across the interface, indicating that no chemical composition gradient exists inside the IMC layer. In Fig. 4c the color gradients are more discernible than in Fig. 4f, indicating that there is a higher gradient of chemical composition across the IMC layer in sample 3.

The SEM images of the joint interface of sample 5 (SS/Al) are provided in Fig. 5a, b. The line scan analysis across the interface along the yellow line shown in Fig. 5b is provided in Fig. 5c. The highlighted yellow regions inside the plot region correspond to IMC layers. In all IMC layers a steep gradient of chemical composition is observed. Moreover, the alloying elements of stainless steel are present in these IMC layers. This implies that not only the Fe atoms, but also the Cr and Ni atoms have diffused into aluminum and remained in the Al–Fe IMC layer. Later in the present paper it will be explained how these alloying elements hinder the interdiffusion rate and reduce the growth kinetics of the IMC layer. The thinner IMC layer in SS/Al joints is attributed to the presence of these elements.

The SEM image of the joint interface of sample 6 (CS/Al) is provided in Fig. 5d, e. A higher volume of IMCs is observed in this sample. The line scan analysis across the interface along the yellow line in Fig. 5e is provided in Fig. 5f. No chemical gradient is observed inside the IMC layer on the left side (corresponding to the streak of IMC layer). A slight gradient is observed inside the IMC layer on the right side (corresponding to the IMC layer in the interface). The chemical gradient inside this layer is 10 units/ μm which is six times smaller than the chemical gradient inside the IMC layer in Fig. 5c which is around 60 units/ μm . Later in this study it will be discussed how a high diffusion rate due to the absence of alloying elements causes a very slight gradient of chemical composition inside the IMC layer. It will also be discussed how the growth rate of IMC layer is pronounced due to a high diffusion rate in CS/Al joints.

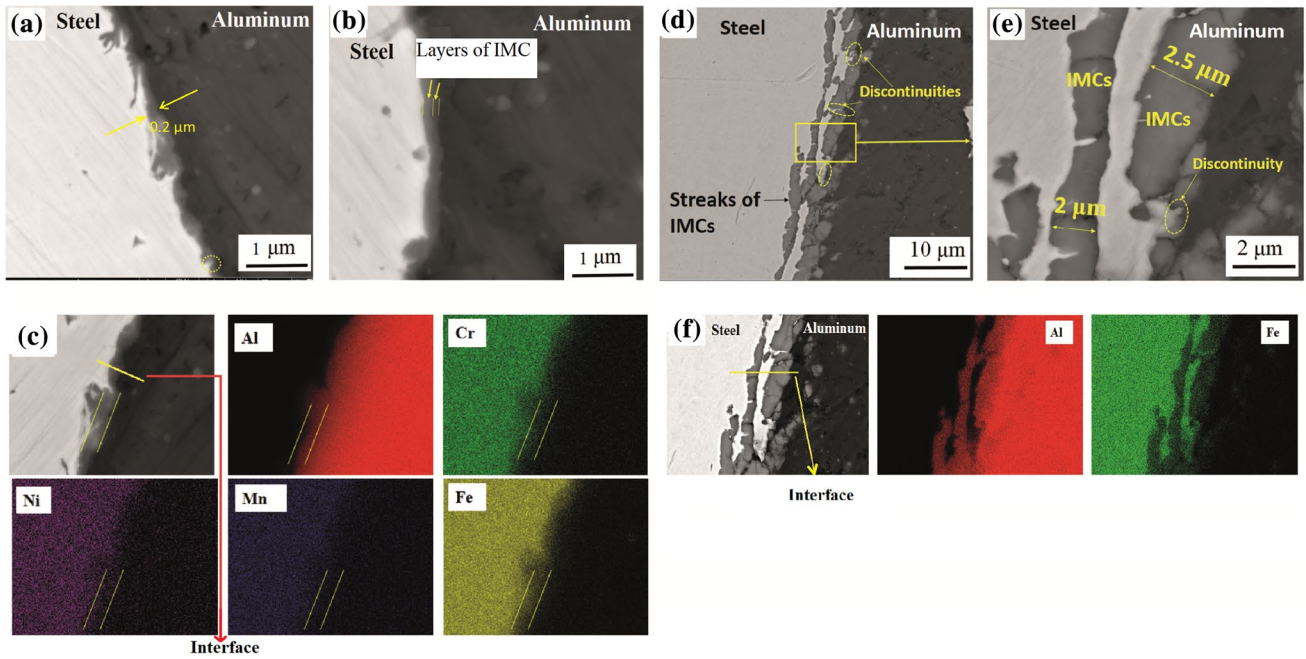
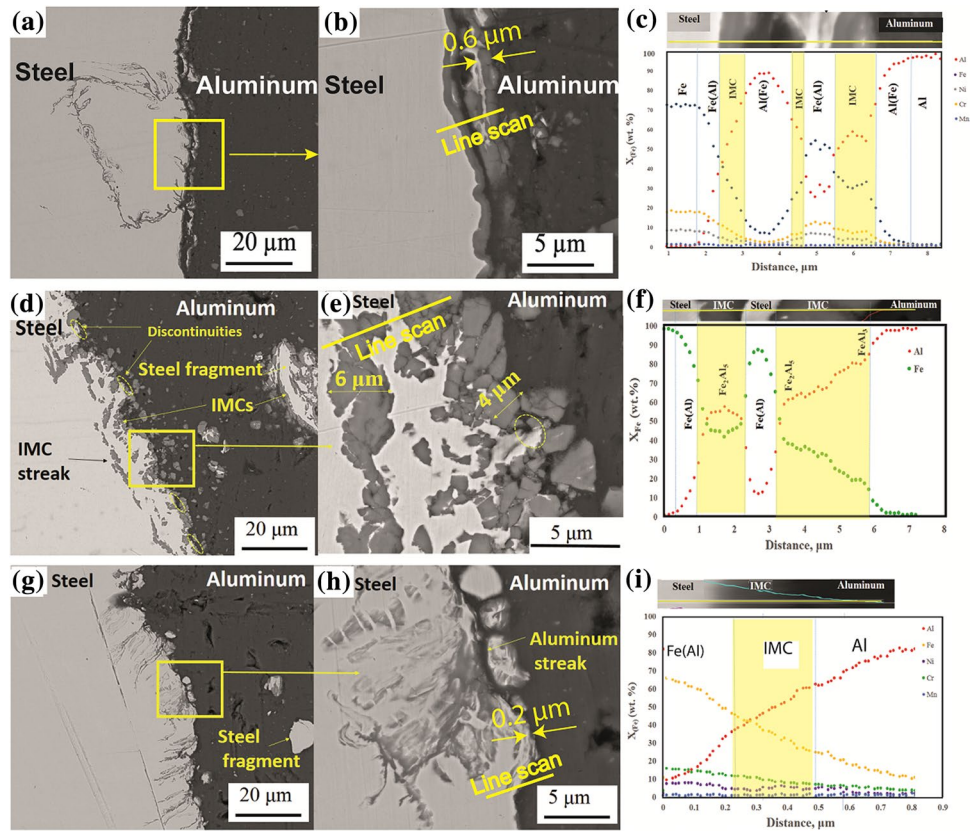


Fig. 4 a, b SEM images from the interface of SS–Al welded joint (No. 3). c The element map analysis of the weld interface (No. 3). d, e SEM images from the interface of CS–Al welded joint (No. 4). f The element map analysis of the weld interface (No. 4)

Fig. 5 a, b SEM image of the joint interface of sample 5. c The line scan analysis across the interface along the yellow line marked in b. d, e SEM image of the joint interface of sample 6. f The line scan analysis across the interface along the yellow line marked in e. g, h SEM image of the joint interface of sample 7. i The highlighted yellow regions are the IMC layers. A high steep of chemical composition gradient is noticeable inside the IMC layers in SS/Al couples. (Color figure online)



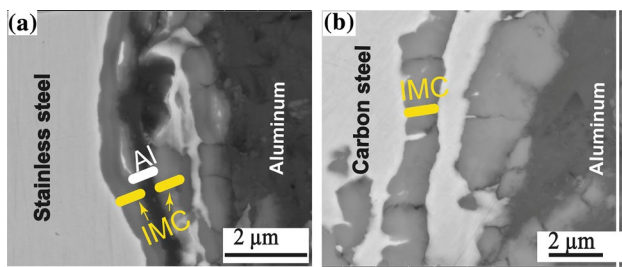


Fig. 6 Higher magnification SEM images from the streaks of **a** SS/Al (sample 5) and **b** CS/Al joints (sample 6). The un-transformed Al layer is clear in the middle of the streak in SS/Al joint. Both welds were performed at 1150 RPM

The SEM images of the joint interface of sample No. 7 (SS/Al) are provided in Fig. 5g and h. It is noticeable how thin the IMC layer at the interface is. Although a higher rotation speed was used during FSW of sample 7 in comparison with sample 5, the thickness of the IMC layer was smaller in sample 7 (0.2 μm in sample 7, 0.6 μm in sample 5). The line scan analysis across the interface along the yellow line in Fig. 5h is provided in Fig. 5i. A high chemical gradient equal to 100 units/ μm is observed inside the IMC layer.

Another distinguishing factor between SS/Al and CS/Al joints is the pattern of streaks in the joint area. Higher magnification images from the streaks observed in SS/Al (sample 5) and CS/Al (sample 6) are provided in Fig. 6a, b, respectively. The streaks in SS/Al joint (Fig. 6a) seems more like a composite structure, composed of 3 layers. The middle layer which is darker is the un-transformed Al streak and the outer layers which are grey are the transformed Al streaks. It means that the diffusion process was not fast enough to convert the middle layer into Fe–Al IMCs. In contrary, the streak in CS/Al joint (Fig. 6b) is a single phase of IMC, indicating that diffusion rate was high enough to convert entire thickness of Al streak into the IMC compound.

As observed in the line scan analyses of Fig. 5, the concentration gradient across the IMC layer in CS/Al joint is almost zero or very low. The most probable IMC in St/Al joints is Fe_2Al_5 . The main reason that this phase is dominant is its higher interdiffusion coefficient with respect to the other IMC phases [37]. Naoi et al. [37] report that the growth rate of IMCs is controlled by diffusion of constitutions. As the interdiffusion coefficient in Fe_2Al_5 is highest among all other possible Fe–Al IMCs, it would be the dominant phase. However, to accurately identify the IMCs present in the interface, Selected Area Diffraction Patterns (SADPs) were taken from different zones of the

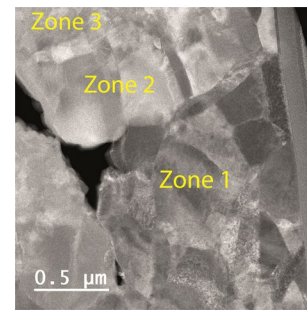


Fig. 7 STEM image of the interface of sample 6. Three different zones are selected to be characterized by TEM and SADP

interface. Figure 7 shows the Scanning Transmission Electron Microscopy (STEM) image taken from the interface of sample 6. The zones where SADPs were taken from are identified in this figure.

Figure 8a, b show the TEM image and the corresponding SADP taken from the zone 1. This zone corresponds to CS analyzed by the incident beam of TEM parallel to $[0\ 0\ 1]$ zone axis. Figure 8c, d show the TEM image and the corresponding SADP taken from the zone 2. This zone corresponds to Fe_2Al_5 analyzed by the incident beam of TEM parallel to $[-\ 1\ 0\ 2]$ zone axis. Figure 8e, f show the HRTEM image and the corresponding Fast Fourier Transformation (FFT) taken from the zone 3. This zone corresponds to $\text{Fe}_4\text{Al}_{13}$ analyzed by the incident beam of TEM parallel to $[1\ 0\ 0]$ zone axis. These analyses confirm that the IMC layer consists of two layers. The sequence of the present phases at the joint interface is Al/ $\text{Fe}_4\text{Al}_{13}$ / Fe_2Al_5 /St.

It was observed that the IMC layers in CS/Al joints were thicker than those ones in SS/Al joints. In addition, as mentioned before, the streaks in CS/Al joints were completely converted into IMCs, while in SS/Al joints they were partially converted into IMCs. This is a critical point in FSW of steel to aluminum as the thickness and morphology of the IMCs determine the bond strength [12, 22]. This difference is attributed to the kinetics of IMC growth. In other words, the kinetics of IMC growth are different for CS/Al and SS/Al couples. In order to know the reason of this difference, an attempt was made in the following to calculate the interdiffusion coefficient in both CS/Al and SS/Al joints.

The interdiffusion coefficient $\tilde{D}(X_{\text{Fe}})$ is composition dependent and the index of X_{Fe} means that it is calculated at a specific composition of Fe. The interdiffusion coefficient is obtained from the equation below [38, 39]:

$$\tilde{D}(X_{\text{Fe}}) = \left[\frac{1}{2.t.\partial X_{\text{Fe}}/\partial x} \right] \cdot \left[Y \cdot \int_{-\infty}^{X_{\text{Fe}}} (X_{\text{Fe}} - X_{\text{Fe}}^{\text{min}}) dx + (1 - Y) \cdot \int_{X_{\text{Fe}}}^{\infty} (X_{\text{Fe}}^{\text{max}} - X_{\text{Fe}}) dx \right] \quad (1)$$

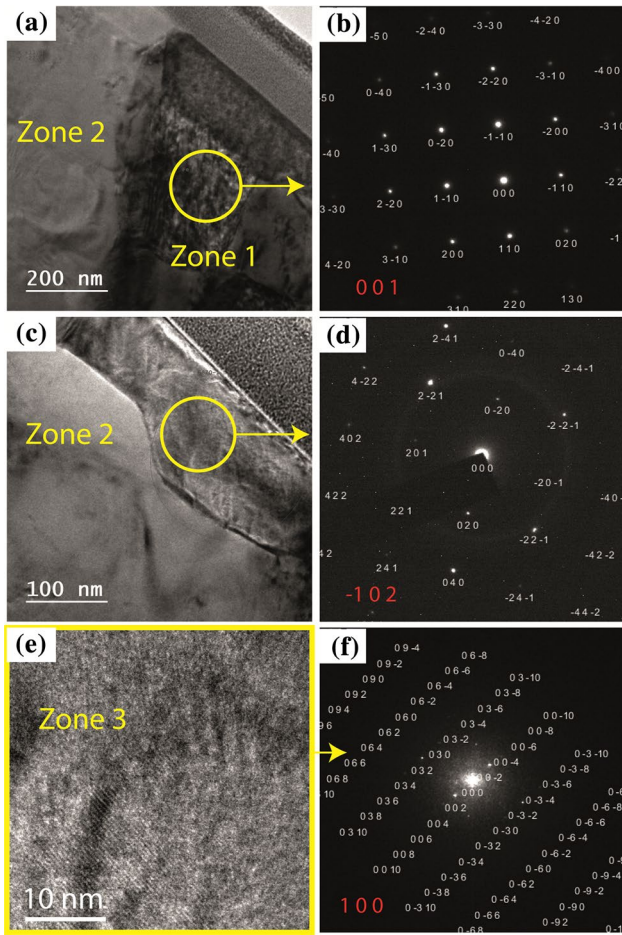


Fig. 8 **a** TEM image taken from the zone 1 and **b** the corresponding SADP showing the [0 0 1] zone axis of CS. **c** TEM image taken from the zone 2 and **d** the corresponding SADP showing the [− 1 0 2] zone axis of Fe₂Al₅. **e** HRTEM image taken from the zone 3 and **f** the corresponding FFT showing [1 0 0] zone axis of Fe₄Al₁₃. The zones were identified in Fig. 7

where

$$Y = \frac{X_{Fe}^{max} - X_{Fe}}{X_{Fe}^{max} - X_{Fe}^{min}} \tag{2}$$

and t and x are time and distance, respectively.

The procedures for calculating the interdiffusion coefficient performed on samples 5 and 6 are illustrated in Fig. 9a, b, respectively. These figures show the concentration of aluminum and iron across the streaks. The interdiffusion coefficients at the interface of steel and IMC layer were computed for both CS and SS and determined to be $14 \times 10^{-14} \text{ m}^2 \text{ s}^{-1}$ and $1.2 \times 10^{-14} \text{ m}^2 \text{ s}^{-1}$, respectively. The interdiffusion coefficients obtained in this study are in the range of the ones reported by Wei et al. [40]. The interdiffusion coefficient in the case of SS/Al is ten orders of magnitude lower than that in CS/Al. This explains why the thickness of IMC in SS/Al joints are lower than CS/Al.

A flat gradient of chemical composition inside the IMC layer in the case of CS/Al joint in Fig. 9b, is another indicative of a high interdiffusion rate. In the case of SS/Al a steep gradient is observed inside the IMC layer, which is an indicative of a lower diffusion rate.

Figure 10 shows the quasi-binary phase diagram of Fe-71 at% Al–Ni which corresponds to the composition of the IMC layer observed in SS/Al joint. The corresponding condition in terms of temperature and composition during FSW is highlighted in this figure. Accordingly, in the conditions present during FSW various Ni-containing phases are stable along with Al–Fe IMCs, such as Al₃Ni₂, Al₁₀Fe₃Ni, and solid solution of BCC_B2. Since only Al–Fe IMCs were detected in this study wherein Ni was present, it can be concluded that Ni is present in a supersaturated solid solution state. This causes a considerable decrease of interdiffusion rate in Al–Fe IMCs, and hence the growth rate of IMCs is hindered.

Figure 11 shows the variation of thickness of IMC layer with respect to the rotation speed during welding. The

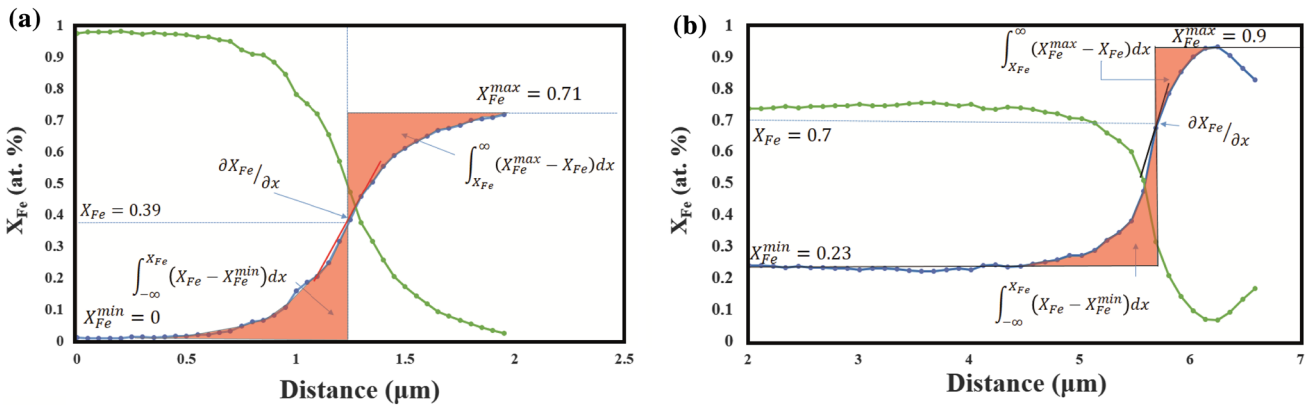


Fig. 9 The procedure of calculating the interdiffusion coefficient in **a** SS–Al (sample 5) and **b** CS–Al (sample 6)

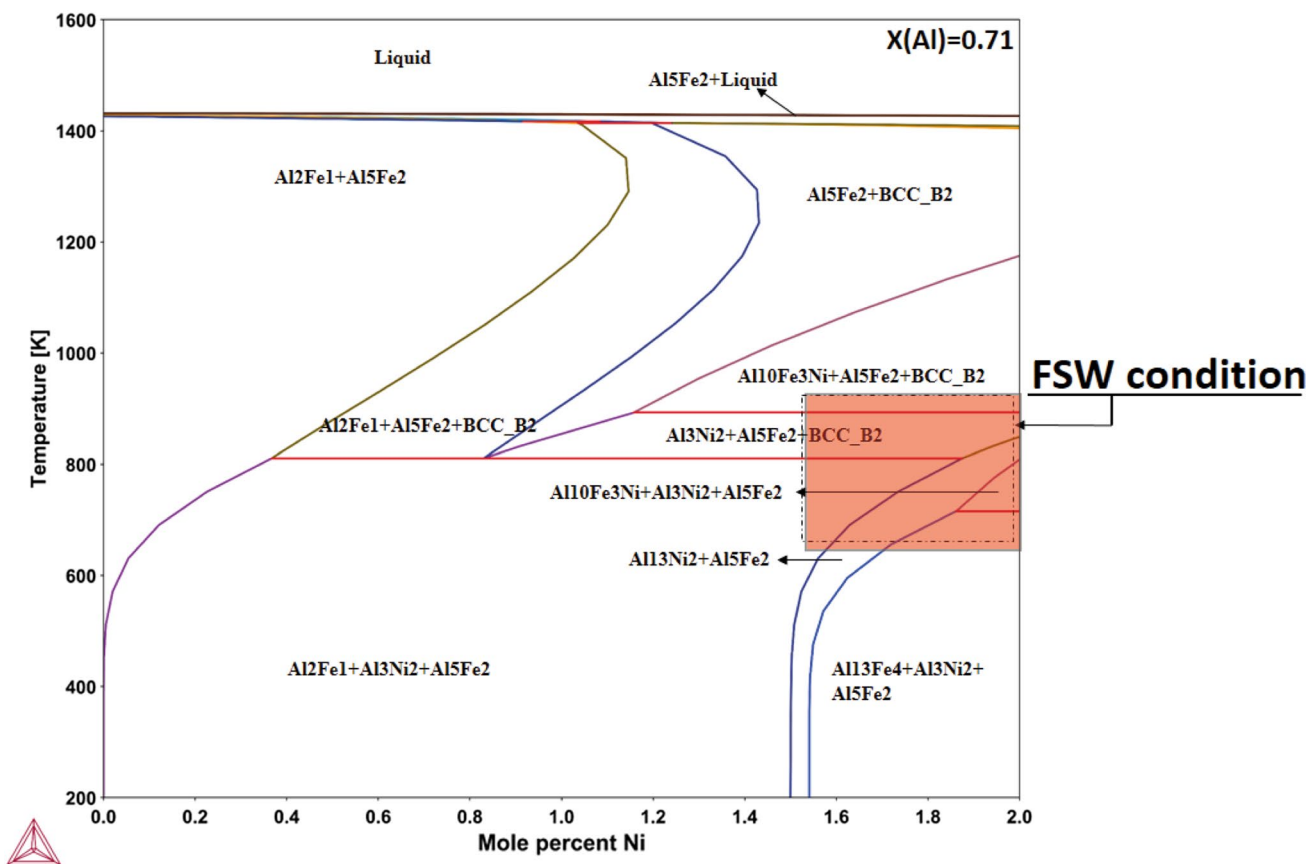


Fig. 10 Quasi-binary phase diagram of Fe-71 at% Al–Ni calculated using Thermo-Calc [41]

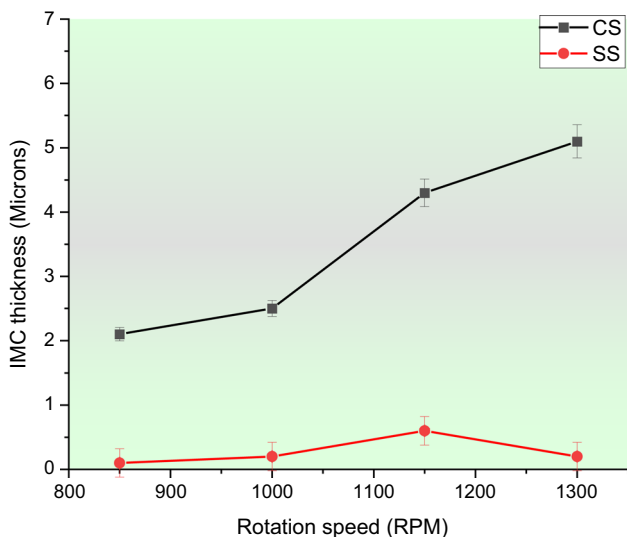


Fig. 11 Variation of the thickness of the IMC layer in CS/Al and SS/Al welded joints with respect to the rotation speed of the tool

difference of the thicknesses of the IMCs in CS and SS joints have been explained. The other difference between CS and SS is the trend of the change of the thickness of the IMCs with respect to the rotation speed. While the thickness of the IMC layer in the CS/Al joint increased by increasing the rotation speed, it began to decline at 1150 RPM in SS/Al joint.

Another distinguishable characteristic in samples 5 and 7 was the observation of several dark branches inside the steel at the interface of the joint. These branches can be observed in Fig. 12a, b which correspond to samples 5 and 7 respectively. Higher magnification images of the branches are provided in Fig. 12c, d. The shape of these features assimilates the intergranular cracks which are usually observed by penetration of low melting liquids into the grain boundaries [42]. EDS analyses taken from steel and the branches are provided in Fig. 12e, f, respectively. Figure 12f shows that these dark branches contain Al, Fe, Cr, and Ni. The presence of all these elements formed a low melting composition which melted during the FSW process and penetrated the grain boundaries of the stainless steel. In fact, observation of these branches is a good evidence of liquation during welding. The lower thickness of the IMC layer at the

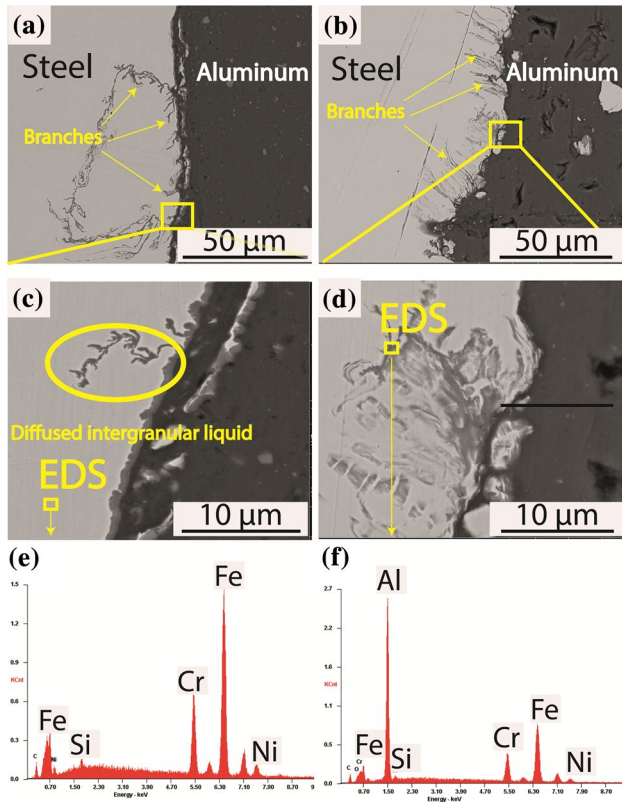


Fig. 12 SEM image taken from the interface of SS/Al from **a** sample 5 and **b** sample 7. **c**, **d** Higher magnification images showing the branches in stainless steel in sample 5 and 7. EDS analyses taken from **e** stainless steel and **f** the branches

interface of sample 7 can be explained by this liquation. At higher rotation speed (1300 RPM) a higher local mixing of both materials occurred in the stir zone. A higher number of branches in sample 7 (Fig. 12b) with respect to sample 5 (Fig. 12a) verifies that a higher rotation speed has led to a higher amount of liquid formation. These branches were rarely seen in samples 1 and 3 in which the rotation speed was lower. The presence of liquid at the interface of the tool and material, where there is an intense mixing, caused a lower coefficient of friction between the tool and material. This reduced the extent of mixing of two materials. As the IMCs nucleate around the rotating tool, at higher rotation speed a lower number of IMCs nucleated, and the overall thickness of the IMC layer was reduced. The liquid that was formed around the rotating pin was finally deposited at the interface. This melt penetrates along the grain boundaries of SS, exhibiting some dark branches observed in Fig. 12. Figure 13a shows the SEM image taken from the interface of sample 7 (SS/Al welded at 1300 RPM) showing a thin IMC due to the liquid formation during FSW. It can be seen in Fig. 13a that some regions at the interface of steel and aluminum are free from IMC layer. The branches in steel which were formed due to the liquation during welding are

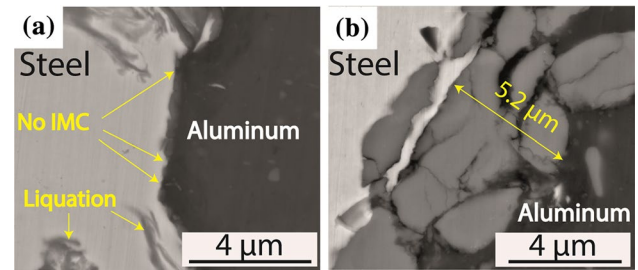


Fig. 13 **a** SEM image taken from the interface of sample 7 (SS/Al at 1300 RPM) showing a thin IMC layer due to the liquid formation during FSW. Some regions are free from IMC layer. **b** SEM image taken from the interface of sample 8 (CS/Al at 1300 RPM) showing a thick IMC layer

observable. Figure 13b shows the SEM image taken from the interface of sample 8 (CS/Al welded at 1300 RPM) showing a thick IMC at the interface. As can be seen no branches are seen in the matrix of carbon steel. The only elements present in this sample were Al and Fe and therefore no low melting compound were formed during mixing of materials.

Figure 14 shows the tensile strengths of CS/Al and SS/Al joints welded at various rotation speeds. All the samples failed from the heat affected zone (HAZ) of Al. A slight variation in the tensile strengths of the joints is related to the degree of softening in HAZ due to the heat effect of the FSW process. Whereas all the samples failed from HAZ and not from the weld interface, it was concluded that IMC layers had no effect on the joint strength. The variation of strength with respect to rotation speed is related to the softening in the HAZ and needs to be analyzed in a separate study. The difference of softening degree in various samples may be

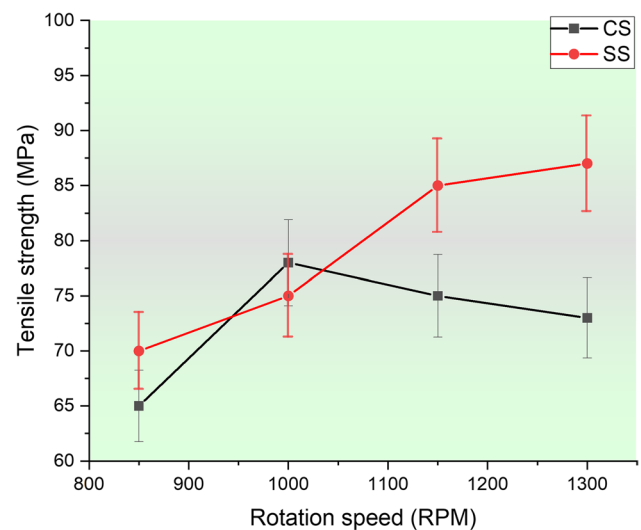


Fig. 14 Tensile strengths of CS/Al and SS/Al joints performed at various rotation speeds of the FSW process

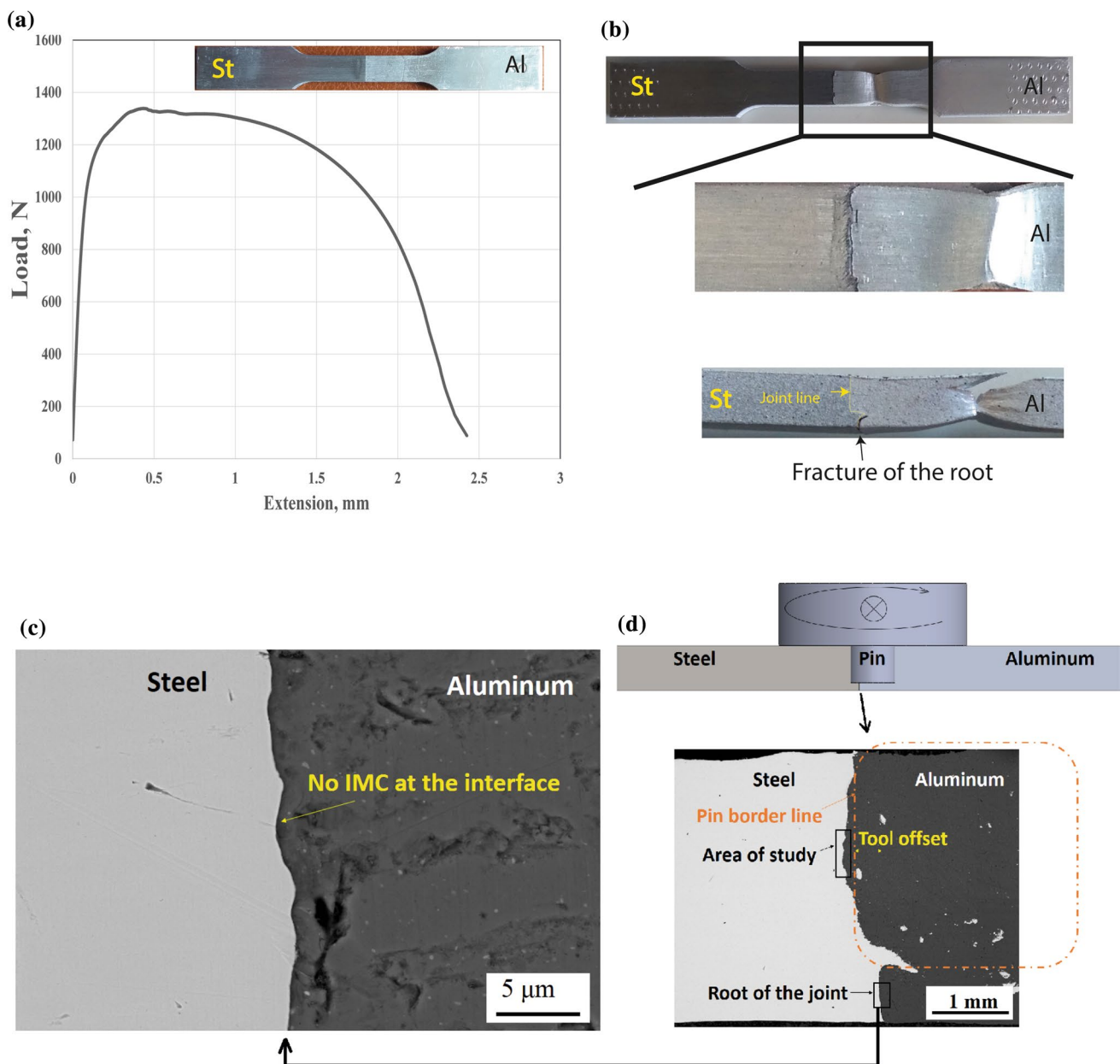


Fig. 15 **a** The load–displacement curve of the sample 6. **b** The tensile specimen after failure. The fracture has occurred from aluminum and a crack is observed in the root weld. **c** SEM image of the root weld

indicating no IMC was formed in the root. **d** The position of the tool relative to the work pieces. There is no contact between the pin and the weld root

attributed to different thermal histories during FSW of SS/Al and CS/Al joint.

In order to analyze the fracture during the tensile test, one of the specimens (sample 6) was studied in more detail. Figure 15a shows the load–displacement curve and Fig. 15b shows the tensile specimen of sample 6 after failure. The specimen failed from Aluminum side and not from the interface of the weld. However, a crack can be observed in the root of the joint (Fig. 15b). The joint efficiency was 100% even though a crack appeared in the root of the joint. To

understand the reason of formation of this crack, the SEM image of the joint line is provided in Fig. 15c. As it can be seen, no IMC layer is observed in the root. This region was placed under the bottom of the pin where there was no contact between the tool and steel. This is because the height of the pin was shorter than the thickness of the sheets (Fig. 15d). The absence of an IMC layer was observed in all CS/Al and SS/Al joints. This implies that a contact between the tool and Steel was a prerequisite for the nucleation of the IMCs. Since there was no contact in

the root, no IMC was formed and consequently no bonding took place in this region. As a crack appeared in this region during the tensile test, it can be concluded that the existence of IMC layer is necessary to establish a joint.

One important result of the present study was that IMCs can only nucleate around the pin in contact with the steel. This is because a localized excess heat was generated between the rotating pin and the steel and this promoted the local interdiffusion of aluminum and steel. Furthermore, the severe stirring action around the pin enhanced the interdiffusion by providing short diffusion paths between aluminum and steel [43].

An illustration of IMC formation and growth in FSW of steel to aluminum is shown in Fig. 16. In section A–A the fragments of steel are detached by the rotating pin and thereby the IMCs nucleate around the pin in the local regions where there is severe mixing of both aluminum and steel. It was observed that in sample 7 the thickness of IMC layer was low. In this sample, lesser number of IMCs nucleated due to the liquation around the pin. This liquation caused a lower coefficient of friction between the tool and material and thereby the extent of severe mixing between two materials decreased. Evidence of this liquation was presented in Fig. 12. In section B–B of Fig. 16 the nucleated IMCs and dispersoids of steel fragments are deposited in the interface of the joint and behind the pin. In section C–C the deposited IMCs begin to grow continuously as long as they are under the influence of the heat of the shoulder. This mechanism is mostly similar to the one proposed by Tanaka et al. [44], with this difference that they stated that the growth of IMCs starts around the rotating pin region. Though the growth of IMC may occur around the rotating pin, severe stirring

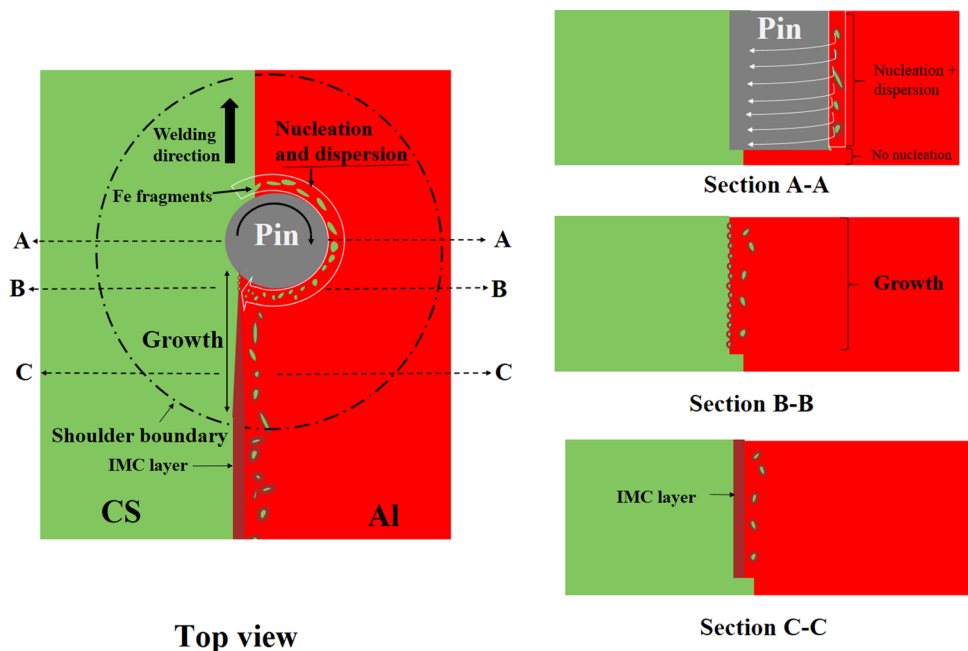
action of the tool disturbs them to fine particles. The continuous growth of IMC begins at the wake of the pin where there is a high temperature under the influence of the rotating shoulder. The big fragments of steel around the rotating tool stop before reaching at the extremity of the rotating pin. These are observable in SEM images in the Al matrix. The observation of detached fragments of steel in the matrix of aluminum is a common observation in FSW of aluminum to steel [45].

4 Conclusions

Two kinds of steels, CS and SS, were friction stir welded to pure aluminum. The kinetics of IMC formation was investigated and the following results were obtained:

1. The overall kinetic of IMC formation in SS/Al joints is lower than CS/Al joints.
2. The IMCs evolution occurs in two separate stages. The nucleation stage takes place around the stirring pin which is in contact with the steel. The growth stage occurs in the interface at the wake of the pin.
3. The thickness of IMC increases with increasing the rotation speed in CS/Al joints while it increases and then decreases in SS/Al joints.
4. At high rotation speed of the FSW tool, the nucleation rate of IMCs in SS/Al joints is lower than CS/Al joints. This is attributed to a liquation which occurs in SS/Al joints due to a low-melting multielement compound of Al–Fe–Ni–Cr.

Fig. 16 An illustration of the Al–Fe IMCs formation and growth during FSW of steel to aluminum. The particles of Fe are rubbed and rotated around the pin (section A–A) and then they are deposited in the wake of the pin (section B–B). During rotation (section A–A) Al–Fe IMCs nucleate and after stopping in the wake of the pin (section B–B) they begin to grow by the influence of the heat of the shoulder (section C–C). No IMC is formed under the shoulder at the root of the joint due to absence of any contact of the pin with steel



5. The interdiffusion coefficient in CS/Al joint is higher than the one in SS/Al joint. This is due to the presence of Ni and Cr in SS which diffuse into IMC layer and reduce the diffusion rate. This causes a lower growth rate of IMCs in SS/Al joints.
6. The root of the joints is free from IMC at the interface which is due to the lack of stirring action and absence of a direct contact between the tool and the steel. These regions are delaminated during the initial stages of the tensile testing.
7. Finally, two factors are responsible for a thinner IMC layer in SS/Al joints. A liquation during FSW and a lower interdiffusion coefficient in SS/Al joint which lead to a lower nucleation rate and a lower growth rate, respectively.

Acknowledgements The authors acknowledge the funding under the reference “UIDP/50022/2020—LAETA—Laboratório Associado de Energia, Transportes e Aeronáutica”.

References

1. A. Khalkhali, E. Miandoabchi, *Thin-Walled Struct.* **157**, 107089 (2020)
2. H. Wang, R. Han, Z. Zhang, M. Zhu, L. Liu, *Mater. Manuf. Process.* **34**, 1671 (2019)
3. L. Shah, M. Ishak, *Mater. Manuf. Process.* **29**, 928 (2014)
4. Y. Zhou, F. Lan, J. Chen, *Thin-Walled Struct.* **49**, 291 (2011)
5. Y. Ge, Y. Xia, *Thin-Walled Struct.* **151**, 106759 (2020)
6. G. Meschut, V. Janzen, T. Olfermann, *J. Mater. Eng. Perform.* **23**, 1515 (2014)
7. M. Graf, S.P. Sikora, C.S. Roider, *Thin-Walled Struct.* **130**, 286 (2018)
8. T. Chen, *J. Mater. Sci.* **44**, 2573 (2009)
9. A.D. D’Souza, S.S. Rao, M.A. Herbert, *Met. Mater. Int.* **26**, 1394 (2020)
10. H. Amaninia, A. Meysami, A. Foroughifar, *Mater. Manuf. Process.* **34**, 1681 (2019)
11. P. Gao, Y. Zhang, K.P. Mehta, *Met. Mater. Int.* **27**, 3085 (2021)
12. R. Beygi, M.Z. Mehrizi, A. Akhavan-Safar, S. Safaei, A. Loureiro, L.F.M. da Silva, *Int. J. Adv. Manuf. Tech.* **112**, 1951 (2021)
13. B. Seo, K.H. Song, K. Park, *Met. Mater. Int.* **24**, 1232 (2018)
14. H. Springer, A. Kostka, E. Payton, D. Raabe, A. Kaysser-Pyzalla, G. Eggeler, *Acta Mater.* **59**, 1586 (2011)
15. M. Pouranvari, *Mater. Sci. Technol.* **33**, 1705 (2017)
16. R.P. Mahto, S. Anishetty, A. Sarkar, O. Mypati, S.K. Pal, J.D. Majumdar, *Met. Mater. Int.* **25**, 752 (2019)
17. P. Prangnell, F. Haddadi, Y. Chen, *Mater. Sci. Technol.* **27**, 617 (2011)
18. S. Madhavan, M. Kamaraj, L. Vijayaraghavan, K. Srinivasa Rao, *Mater. Sci. Technol.* **33**, 200 (2017)
19. L. Wan, Y. Huang, *Int. J. Adv. Manuf. Tech.* **99**, 1781 (2018)
20. P. Karakizis, D. Pantelis, D. Dragatogiannis, V. Bougiouri, C. Charitidis, *Int. J. Adv. Manuf. Tech.* **102**, 3065 (2019)
21. K.P. Mehta, *J. Mater. Res.* **34**, 78 (2019)
22. R. Beygi, M. Kazeminezhad, A. Kokabi, A. Loureiro, *Metal. Mater. Trans. A* **46**, 2544 (2015)
23. R. Beygi, M.Z. Mehrizi, D. Verdera, A. Loureiro, *J. Mater. Eng. Perform.* **255**, 739 (2018)
24. R. Beygi, M.A. Kazeminezhad, A. Kokabi, *Trans. Nonferrous Met. Soc. China* **22**, 2925 (2012)
25. R. Beygi, M. Kazeminezhad, A. Kokabi, *Metal. Mater. Trans. A* **45**, 361 (2014)
26. M. Thomä, A. Gester, G. Wagner, M. Fritzsche, *Metals* **10**, 1079 (2020)
27. P. Kaushik, D.K. Dwivedi, *J. Manuf. Process.* **68**, 198 (2021)
28. R.P. Mahto, S.K. Pal, *J. Manuf. Process.* **55**, 103 (2020)
29. B.-S. Sung, H.-S. Bang, S.-O. Jeong, W.-S. Choi, Y.-H. Kwon, H.-S. Bang, *Met. Mater. Int.* **23**, 562 (2017)
30. F. Liu, P. Dong, *Scripta Mater.* **191**, 167 (2021)
31. M. Moradi, M.S. Meiabadi, V. Demers, *Int. J. Prod. Res.* **16**, 32 (2021)
32. A. Wierzbicka-Miernik, K. Miernik, R. Filipek, K. Szyszkiewicz, *J. Mater. Sci.* **52**, 10533 (2017)
33. K. Zhang, X. Bian, Y. Li, Y. Liu, C. Yang, *J. Mater. Res.* **28**, 3279 (2013)
34. A.M. Milani, M. Paidar, A. Khodabandeh, S. Nategh, *Int. J. Adv. Manuf. Tech.* **82**, 1495 (2016)
35. M. Vahdati, M. Moradi, M. Shamsborhan, *Trans. Indian Inst. Met.* **73**, 2587 (2020)
36. Z. Shen, Y. Chen, M. Haghshenas, A. Gerlich, *Eng. Sci. Technol.* **18**, 270 (2015)
37. D. Naoi, M. Kajihara, *Mater. Sci. Eng. A* **459**, 375 (2007)
38. F. Sauer, V. Freise, *Z. Elektrochem.* **66**, 353 (1962)
39. H. Mehrer, *Diffusion in Solids: Fundamentals, Methods, Materials, Diffusion-Controlled Processes* (Springer, Verlag Berlin Heidelberg, 2007)
40. Y. Wei, J. Xiong, J. Li, F. Zhang, S. Liang, *Mater. Sci. Technol.* **33**, 1208 (2017)
41. J.-O. Andersson, T. Helander, L. Höglund, P. Shi, B. Sundman, *Calphad* **26**, 273 (2002)
42. C. Dharmendra, S. Shakerin, G.J. Ram, M. Mohammadi, *Materialia* **13**, 100834 (2020)
43. N. Kulkarni, W. Yuan, R.S. Mishra, *Friction Stir Welding of Dissimilar Alloys and Materials* (Butterworth-Heinemann, Oxford, 2015)
44. T. Tanaka, M. Nezu, S. Uchida, T. Hirata, *J. Mater. Sci.* **55**, 3064 (2020)
45. P. Goel, N.Z. Khan, Z.A. Khan, A. Ahmari, N. Gangil, M.H. Abidi, A.N. Siddiquee, *Mater. Manuf. Process.* **34**, 192 (2019)

Publisher's Note Springer Nature remains neutral with regard to jurisdictional claims in published maps and institutional affiliations.